

See discussions, stats, and author profiles for this publication at: <https://www.researchgate.net/publication/231706356>

# Small-Angle X-ray Scattering on Melt-Spun Polypropylene Fibers: Modeling and Data Reduction

ARTICLE in MACROMOLECULES · MAY 2010

Impact Factor: 5.8 · DOI: 10.1021/ma902414b

---

CITATIONS

3

---

READS

37

## 4 AUTHORS, INCLUDING:



Othmar Marti

Universität Ulm

281 PUBLICATIONS 5,416 CITATIONS

SEE PROFILE

## Small-Angle X-ray Scattering on Melt-Spun Polypropylene Fibers: Modeling and Data Reduction

Stefan Fischer,<sup>\*†</sup> Othmar Marti,<sup>‡</sup> Tobias Diesner,<sup>‡</sup> and Bernhard Rieger<sup>‡</sup>

<sup>†</sup>Institute of Experimental Physics, University of Ulm, Ulm, Germany, and <sup>‡</sup>Wacker-Lehrstuhl für Makromolekulare Chemie, Technische Universität München, Garching, Germany

Received October 31, 2009; Revised Manuscript Received April 21, 2010

**ABSTRACT:** We present a method for the evaluation of SAXS data of highly oriented semicrystalline polymers, allowing us to determine up to seven structural parameters from the measurements. The utilized samples were polypropylenes with varied distributions of the molecular weight, which were spun with different take-up velocities to alter the spinline stress, thus influencing the structural properties. We were able to determine the degree of orientation, lamella radius, long spacing, lattice distortion, and lamella height simultaneously. The microscopic orientation was compared with the crystalline orientation evaluated by Herman's orientation function from WAXS.

### Introduction

Isotactic polypropylene (PP) is among the most widely used polymers, possessing a wealth of different properties.<sup>1</sup> A difficult interplay among molecular structure, morphology, and processing conditions determines the end-use properties.<sup>1,2</sup>

A typical morphological structure in PP is the so-called shish-kebab structure (Figure 1). Depending on the actual processing conditions, a shish-kebab can occur when the melt is submitted to a mechanical deformation or stress: Few parallel chains (stretched over several 100 nm) build the backbone and serve as a nucleation site for a secondary crystallization, leading to a lamella like epitaxial growth.<sup>3–8</sup> Additional crystals (which are not shown in the Figure) can grow perpendicular on the lamellas (kebabs).<sup>9–11</sup> The first description of such a morphology in melt spun fibers has been given by Dees and Spruiell.<sup>12</sup>

A convenient way to analyze the structure of bulk polymers like the shish-kebab or semicrystalline structure is X-ray scattering. Using wide- and small-angle setups, we can determine structures in the range of a few angstroms to ~100 nm. This covers the crystalline properties (wide-angle x-ray scattering, WAXS) as well as the lamellar range (small-angle x-ray scattering, SAXS). In general, the scattering amplitude is the Fourier transform of the electron density variation in the sample. During the recording process, the phase information of the scattered wave is lost. Therefore, we cannot directly calculate the actual morphology of the sample from the scattering image. There are several methods known for interpreting and analyzing scattering images.<sup>13–16</sup> A promising approach is to develop a model of the assumed structure (Figure 1), calculate the scattering intensity, and then fit the model to the actual scattering distribution. Simulations with such models also help to better understand the morphology of the sample and the scattering results.

In situ and ex situ X-ray scattering on melt-spun fibers, especially regarding the orientation of the crystalline regions, has been extensively interpreted before. Usually, Herman's orientation function has been analyzed on WAXS data to determine the chains alignment in polymers like polyethylene,<sup>4,12,17</sup> PP,<sup>11,18–21</sup>

nylon,<sup>22,23</sup> polyethylene naphthalate,<sup>24</sup> or poly(oxymethylene).<sup>25</sup> A review comparing the different polymers has been published by White and Cakmak.<sup>26</sup> Most of the studies named above include SAXS measurements. The analysis of those usually has been restricted to the qualitative comparison of the scattering images,<sup>17,19,20,22,26–29</sup> a peak analysis to determine the long spacing,  $L$  (Bragg),<sup>7,11,18,24,30,30–33</sup> Guinier approximation or Scherrer evaluation of the lamella size,<sup>11,25</sup> the total scattering intensity,<sup>21</sup> or the analysis of the 1D correlation function.<sup>4,25</sup>

To analyze SAXS data from as-spun iPP-fibers, we used a model proposed by Wilke for partially oriented polymers<sup>34–41</sup> based on previous considerations by Deas<sup>42</sup> and adapted it to our samples. By evaluating the actual scattering data with this model, we gain up to seven parameters describing the structure of the fibers. Usual approaches only give long spacing and height of the lamellas. In addition, we can analyze lattice distortion, lamella diameter, and the general degree of orientation with our approach. We also evaluated Herman's orientation factor from WAXS measurements to compare lamellar and crystalline orientation.

White et al. identified the spinline stress to be the significant parameter for orientation, crystallinity, and mechanical properties of spun fibers.<sup>19</sup> The spinline stress can be increased by lower flow rates (higher viscosity via molecular weight or reduced temperature) and higher take-up speeds. To test our model for different spinline stresses, we used two PPs with different distributions of the molecular weight at different take-up velocities.

### Experimental Section

**Materials and Sample Preparation.** The utilized PPs are given in Table 1. For melt spinning, we used a low-molecular-weight polymer (“matrix”) as well as a blend of 20% high molecular weight PP with the low molecular material (“blend”).<sup>43</sup> After insertion of the respective polymer in the extruder, the temperature was increased over the melting temperature to 250 °C using a nitrogen atmosphere to prevent oxidation. The components were then mixed by a worm gear at 50 rpm for 10 min with material backflow. Afterward, the melt was cooled to 200 °C while continuously mixing. After ~15 min, the polymers were extracted from the extruder as fibers. The spinning speed was varied, thus leading to different diameters of the fibers. One sample of each

\*To whom correspondence should be addressed. E-mail: stefan.fischer@wirtschaftsphysik.de.

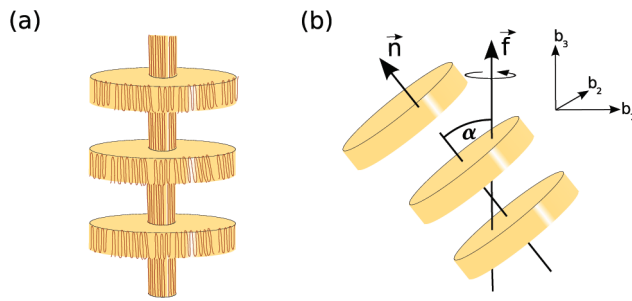


**Figure 1.** (a) Shish-kebab structure. (b) Model depiction of the scattering objects (here: cluster of crystalline cylinders in an amorphous matrix), which can be tilted in relation to the fiber axis,  $\vec{f}$ , under an angle,  $\alpha$ . The cylinders themselves might be tilted toward the cluster normal,  $\vec{n}$ , at an angle,  $\Phi$ .

**Table 1. Used Polypropylenes for Blending and Fiber Spinning**

polymer	$M_w$ (g/mol)	polydispersity	$T_m$ (°C)	tacticity [mmmm] (%)
low molecular	250 000	4.8	168	> 98
high molecular	1 100 000	4.5	158	> 96

polymer (matrix and blend) was prepared as direct flow from the extruder without melt-spinning. The spinning was done by a paddle with a diameter of 6.2 cm, which was attached to a drill with 10 different rotational frequencies. To introduce the “direct flow” fibers in the Figures, we calculated a “virtual” take-up velocity according to their diameter from an exponential fit to a velocity–diameter diagram. We attributed  $v = 15$  mm/s to the matrix polymer and  $v = 9.5$  mm/s to the blend.

**WAXS Measurements.** WAXS experiments have been performed in flat film and Guinier setup on a Philips PW1830 instrument with vertical anode arrangement. The  $K_\alpha$  line of the water-cooled copper anode was selected with a nickel filter for the 2D measurements and by Bragg reflection monochromatization in the Guinier setup. Measurements were done in vacuum to avoid background scattering on air molecules. We used BaFBr/Eu<sup>2+</sup> image plates to record the scattering. The image plates were read out with a FujiFilm fluorescent image analyzer (FLA-3000 series).

The Guinier setup is based on a focusing, high-intensity crystal monochromator and an eccentric cylinder chamber and was used to determine the scattering profile. Samples are rotated during the measurement to rule out the effects of orientation. The crystalline fraction in the polymers can be detected from these measurements by comparing the areas under the amorphous ( $A_A$ ) and semicrystalline ( $A_{\text{total}}$ ) curve. For this purpose, only the scattering from the first peak to the middle between first and second halo is considered.<sup>15,16</sup> The scattering curve of the amorphous fraction was determined from a completely amorphous PP sample. The crystalline fraction,  $X_C$ , then becomes  $X_C = (A_{\text{total}} - A_A)/A_{\text{total}}$ . The Guinier measurements also showed the typical scattering profile of the monoclinic  $\alpha$ -modification.<sup>1</sup>

A flat-film chamber was used to measure 2D WAXS. Flat film results can be used to determine the degree of orientation in the crystalline areas of our polymers. For this purpose, usually the Herman’s orientation factor is calculated. In principle, the azimuthal intensity profile of the different lattice planes is developed into orthogonal Legendre polynomials  $P_n(\cos \phi)$ .<sup>44</sup> The second expansion coefficient without the prefactor is used as Herman’s orientation function,  $f$

$$f = \langle P_2(\cos \phi) \rangle = \frac{1}{2} (2\langle \cos^2 \phi \rangle - 1) \quad (1)$$

with

$$\langle \cos^2 \phi \rangle = \frac{\int_0^{\pi/2} I(\phi) \cos^2 \phi \sin \phi d\phi}{\int_0^{\pi/2} I(\phi) \sin \phi d\phi}$$

From the scattering images, we can calculate the orientation of the (110), (040), and (130) lattice planes, which are needed to determine the orientation of the crystallographic axes. The factor  $f_{040}$  can be used directly as the orientation factor of the  $b$  axis,  $f_b$ . In monoclinic PP, the chains in their helical conformation are aligned along the  $c$  axis. Because there is no convenient scattering to determine the orientation of the  $c$  axis, Wilchinsky’s method<sup>45</sup> has to be used to calculate  $f_c$ :  $f_c = -1.099f_{110} - 0.901f_{040}$ . For orthogonal axes, we find  $f_d + f_b + f_c = 0$ .<sup>46</sup> Because the actual  $a$  axis is not perpendicular to the  $c$  axis in monoclinic PP, it is convenient to define an  $a'$  axis.<sup>11,19</sup> The resulting parameters  $f$  range from  $-0.5$  to  $1$  with  $f = -0.5$  meaning that the normal vectors of the lattice planes are perpendicular to the fiber axis,  $f = 0$ , meaning that the normal vectors are statistically oriented (isotropic orientation), and  $f = 1$ , meaning that the normal vectors of the lattice are aligned parallel to the fiber axis. More details of this approach can be found in literature.<sup>16,44,45</sup>

**SAXS Measurements.** For SAXS measurements, we used a Bruker ASX Nanostar with a Cu-anode X-ray generator, operating in vacuum at the  $K_\alpha$  line. The beam is monochromatized and collimated by cross-coupled Goebel mirrors and a three-pinhole collimation system. The scattered data were recorded at a sample–detector distance of 1056 mm with a 2D position-sensitive Bruker HiStar detector with a pixel size of 112.3  $\mu\text{m}$ . A measurement of the scattering background was performed and subtracted from each scattering image.

The utilized model for the simulation and evaluation of the scattering of oriented structures has been proposed by Wilke,<sup>34,35,38</sup> based on previous work by Deas,<sup>42</sup> and adapted to the analyzed structures. An overview over the complete calculations is given in Figure 2. The mathematical basics are presented below. First, we show how to introduce orientation of given scattering units and then define the actual cluster structure.

To introduce an orientation function, we assume that the scattering units (clusters) show orientation along a given direction,  $\vec{f}$  (fiber axis). The scattering units have to fulfill the following assumptions:<sup>34,35,42</sup> (1) The scattering units (clusters) have a rotational symmetry around a vector  $\vec{n}$ , which is defined as the clusters normal vector. (We will later assume that the scattering units are lamella stacks or kebabs in semicrystalline polymers.) (2) The normal vector,  $\vec{n}$ , shows a rotational symmetry to the fiber axis,  $\vec{f}$ . (3) The normal vector  $\vec{n}$  can be tilted with regard to the fiber axis (indicated in Figure 1) with a mean angle,  $\alpha_0$ , and a variance of  $\sigma$ , resulting in a probability density function  $D(\alpha)$ .

The scattering intensity,  $I_C$ , of one scattering unit is  $I_C(\vec{q}) \propto |\mathcal{F}(\rho(\vec{r}))|^2$  with  $\rho(\vec{r})$  as the density distribution in the scattering cluster and  $\mathcal{F}$  denoting the Fourier transformation.<sup>13,16</sup> In spherical coordinates  $\vec{b} = (r^*, \phi^*, \theta^*)$  we find the Legendre expansion coefficients  $G_{2n}^0$  of  $I_C$

$$G_{2n}^0(r^*) \equiv \frac{4n+1}{4} \int_0^\pi d\theta^* \sin \theta^* \int_0^{2\pi} d\phi^* I_C(r^*, \phi^*, \theta^*) P_{2n}(\cos \theta^*) \quad (2)$$

The probability density function  $D(\alpha)$  of the scattering units around the fiber axis similarly can be expanded to

$$D_{2n} \equiv \frac{4n+1}{2} \int_0^\pi d\alpha \sin \alpha D(\alpha) P_{2n}(\cos \alpha)$$

We finally get the scattering intensity of partially oriented scatterers via

$$I(r^*, \theta^*) = \sum_{n=0}^{\infty} \frac{2}{4n+1} D_{2n} G_{2n}^0(r^*) P_{2n}(\cos \theta^*) \quad (3)$$

The detailed derivation leading to equation eq 3 can be found in Deas’s work.<sup>42</sup>

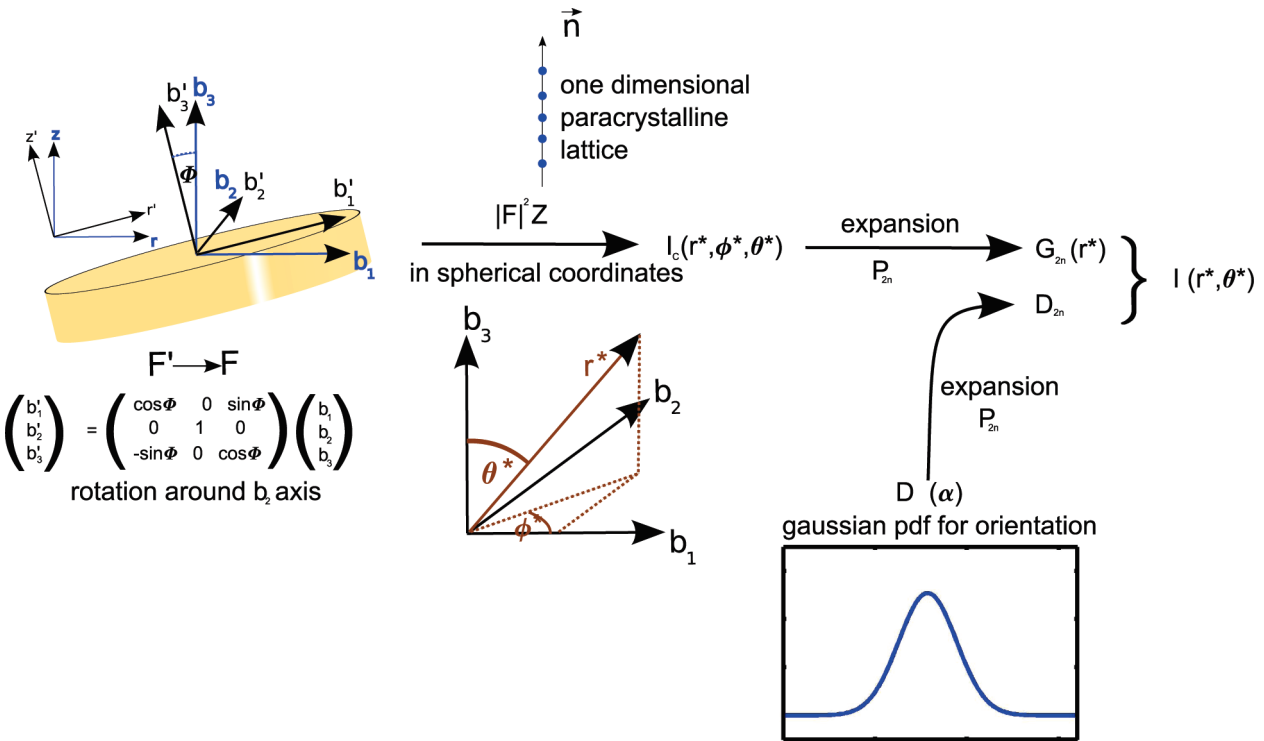


Figure 2. Derivation pathway of the scattering of oriented clusters.

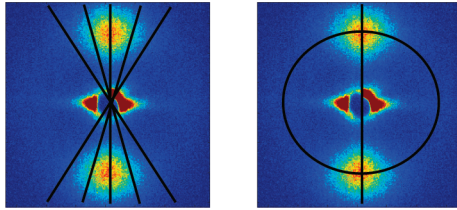


Figure 3. The evaluation method proposed in literature is depicted in the left image by the dotted lines. A faster evaluation with higher accuracy is achieved by evaluating on the azimuthal slice and the meridian slice (right image).

The presented approach shows several advantages: (1) We can separate orientation ( $D_{2n}$ ) and structure ( $G_{2n}^0$ ) of the scattering units. (2) Usually, we find that the number of coefficients,  $D_{2n}$ , is small; therefore, we only have to expand  $I_C$  to its first orders in  $G_{2n}^0$ . (3) The scattering units can show a variety of structures because we have only few constraints.

Moreover, eq 3 shows that despite the complicated calculations, we only have to evaluate one expansion coefficient  $G_{2n}^0$  for a fixed  $r^*$ . Prior publications used several slices through the scattering data to which the model was fitted (Figure 3).<sup>38,40</sup> We found that analyzing the data first on the  $b_3$  axis and then on an azimuthal slice for a fixed distance from the scattering center enables us to speed up the fitting process by a factor of 10 to 50.<sup>47</sup>

To analyze orientation and dimension of a lamellar or shish-kebab structure (Figure 1) from SAXS, we assume that the scattering units consists of cylinder-like crystallites (lamellas or kebab) embedded in an amorphous matrix, as already indicated in Figure 1. Crystalline and amorphous layers alternate in a 1D paracrystalline lattice, as described by Hosemann,<sup>48–50</sup> forming clusters at which the X-rays are scattered.

The utilized model for the scattering units includes the possibility that the cylinders are tilted at an angle  $\Phi$  toward the cluster normal,  $\vec{n}$ . The cylinders have a height,  $H$ , a radius,  $R$ , and a spacing (long period),  $L$ . The scattering intensity of such a cluster is

in principle

$$I_C = |F|^2 Z^* |S|^2 \quad (4)$$

The single factors of  $I_C$  are the scattering amplitude,  $F$ , of a single cylinder, the lattice factor,  $Z$ , for a lattice with infinite range in the  $b_3$  direction and a correction factor,  $|S|^2$ , for a finite lattice of  $N$  lamellas (cylinders), which is applied via a convolution.<sup>35</sup>

The utilized coordinate systems have already been introduced in Figures 1 and 2. To calculate the scattering amplitude of a cylinder with radius,  $R$ , and height,  $H$ , we start in cylindrical  $\vec{b}'$  coordinates<sup>13,51</sup>

$$F(b'_r, b'_3) = \mathcal{F}\{\rho(r', z')\}$$

$$= \pi R^2 H \frac{2J_1(2\pi Rb'_r)}{2\pi Rb'_r} \frac{\sin(\pi Hb'_3)}{\pi Hb'_3} \quad (5)$$

with  $b'_r = (b'_1^2 + b'_2^2)^{1/2}$  and  $J_1$  denoting a Bessel function of the first kind and first order. A simple rotation of the primed coordinate system around the  $b'_2$  axis by an angle  $\Phi$  accounts for tilted lamellas and yields in the  $\vec{b}$  system.

In  $\vec{b}$  coordinates, we multiply the scattering amplitude with the lattice factor  $Z(b_3)$ . The lattice factor of a paracrystalline lattice with a Gaussian distribution of the lattice spacing is<sup>38,40,48</sup>

$$Z(\bar{b}_3) = \frac{1 - |h(\bar{b}_3)|^2}{1 + |h(\bar{b}_3)|^2 - 2|h(\bar{b}_3)|\cos(2\pi\bar{b}_3\bar{L})} \quad (6)$$

with  $\bar{L}$  as the (mean) lattice spacing. In the above given literature, one finds  $|h(\bar{b}_3)| = e^{-1/2(2\pi g\bar{b}_3\bar{L})^2}$  where  $g = \Delta L/\bar{L}$  (with  $\Delta L = (\langle(L - \bar{L})^2\rangle)^{1/2}$ ) denotes the lattice distortion parameter.<sup>52</sup>

For the simulations and fits, we reduced the number of parameters to enhance the computation speed. It has been shown by Wilke, Fronk, and Göttlicher,<sup>35,37–40</sup> that the finite size of the clusters (and therefore finite number of cylinders) can usually be neglected for  $> 10$  crystallites. AFM measurements on sheared thin films of polyethylene suggest that the number of kebabs is significantly higher.<sup>53</sup> If the number of crystallites is

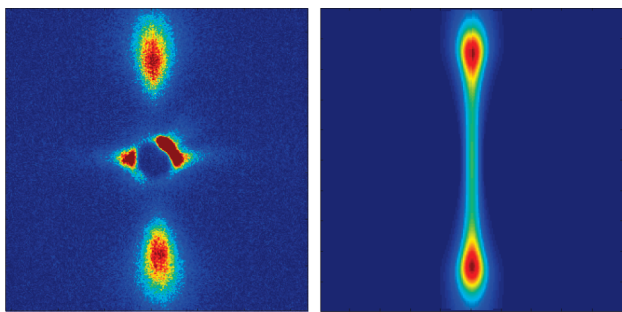


**Figure 4.** Comparison of original data and simulation.

lower, then the resulting scattering can be approximated with a higher lattice distortion factor,  $g$ . We therefore omitted the factor  $*|S|^2$  in eq 4.

We used a normal distribution for the orientation function  $D(\alpha)$  with the parameters  $\alpha_0$  for a given mean orientation and  $\sigma$  for the variance of the distribution. For data evaluation we set  $\alpha_0 = 0$  and  $\Phi = 0$  because we do not expect a tilting of the kebabs in relation to the shish or of the shish-kebabs toward the fiber axis.

The presented model uses some implicit assumptions for the scattering units, which have not been addressed yet. The following simplifications have been made for computational reasons, reducing the number of free parameters: (a) Radii and heights of the lamellas are assumed to be constant; in reality, we would expect size distributions for both. (b) The transition from crystalline to amorphous regions is rather abrupt; lamellar structures usually show a transition zone. (c) We used a Gaussian distribution for the orientation of the clusters; a more general choice would be a Parson VII function, which also allows long tails by including a third parameter. Despite these limitations of the underlying model, the parameters obtained from data fitting should still provide valuable insight into the polymers structure.

To speed up data evaluation, lamella spacing,  $L$ , lamella height,  $H$ , and lattice distortion,  $g$ , were analyzed on the meridian with a simplified model of cylinders in a 1D, paracrystalline lattice.<sup>54</sup> Lamella radius,  $R$ , and degree of orientation,  $\sigma$ , were then fitted with the complete model calculation on an azimuthal slice. The azimuth fits were performed on the radius of the highest intensity from the orientation scattering because there the signal-to-noise ratio is best. Error analysis has been performed as follows: For the data reduction along the meridian (regarding long spacing, height, and lattice distortion of the lamella clusters), we took the  $2\sigma$  confidence intervals (95%), as calculated by the fitting algorithm. For the azimuthal slices, we found that radius and degree of orientation show an (experimental) correlation, originating in the influence of the take-up velocity both on orientation and lamella width. As a consequence, the confidence interval can become (unphysically) big.<sup>55</sup> We therefore fitted 10 slices through the meridional scattering peak adjacent to the maximum position (in  $\Delta q = 0.1 \text{ 1/nm}$  steps) and calculated mean and standard deviation for the respective samples.

Figure 4 shows measured data that have been fitted and a simulation with the respective fit parameters. Whereas the simulated scattering between the two lobes is an artifact from the limitations of the model (assumptions of a sharp transitions between amorphous and crystalline phase and infinite cluster sizes), the general shape of the two lobes is reproduced correctly. This confirms the validity of our approach.

More simulations regarding the influence of the different model parameters are included in the online supplement. It should be noted that prior publications used Herman's orientation parameter or simply the SAXS azimuthal breadth<sup>56</sup> to compare the degree of orientation in elongated or fiber spun semicrystalline polymers. The width of the broadening of the meridional reflex perpendicular to the fiber or stretching

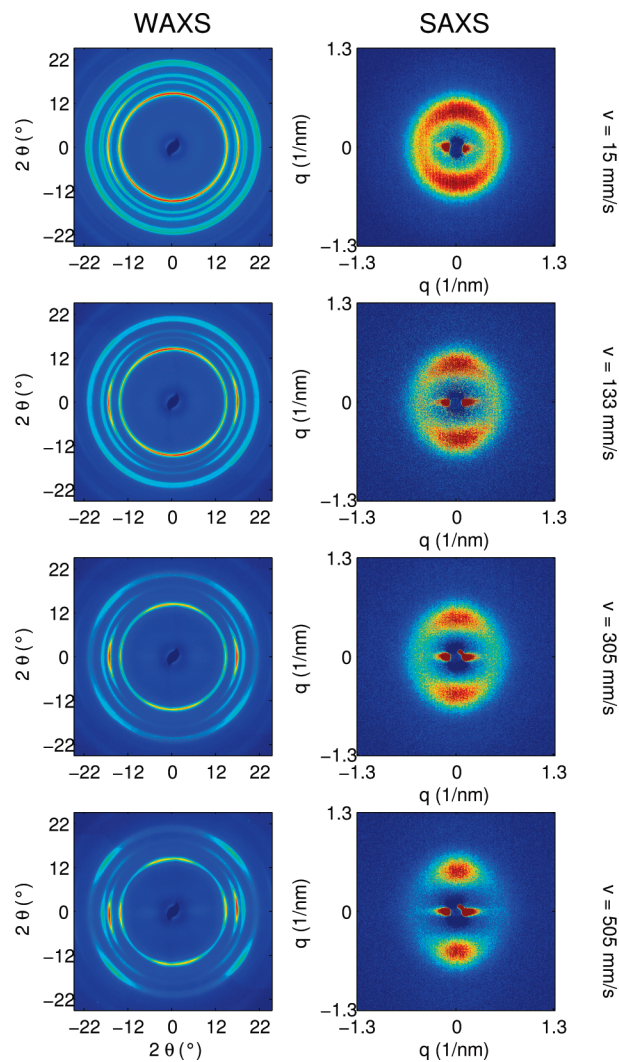


**Figure 5.** Examples of WAXS and SAXS measurements at polymer fibers with different take-up speeds. The polymer used for fiber spinning was the “matrix sample”.

direction has been used before to determine the lateral size of the lamellas. This approach is only valid if the scattering units are perfectly oriented, and the scattering does not spread into an arc.<sup>57,58</sup> The here presented model in contrast distinguishes between the influences of orientation and lateral dimension (radius) of the scattering units.

## Results

**SAXS Orientation in Melt-Spun Polypropylenes.** An overview on the measured SAXS data is given in Figures 5 (matrix sample) and 6 (blend sample). Especially for faster spinning velocities, we can clearly identify a narrowing of the peaks on the meridian. Those peaks originate in the kebab structure of the samples. At most samples, we also identify an equatorial streak. This pattern is consistent with a shish-kebab structure, as described in the literature.<sup>3,10,11</sup>

Figure 7 shows that neither the long period,  $L$ , nor the lamella height,  $H$ , have clear trends for different take-up speeds, especially in the blend. The lattice distortion,  $g$ , however is reduced with increasing take-up velocities. A similar effect has already been described for polyethylene<sup>12</sup> and nylon 6 fibers.<sup>59</sup> There, Bragg's law and (in the case of nylon) the 1D correlation function have been used to evaluate  $L$  and  $H$ . The lattice distortion cannot be computed with the approach used there.

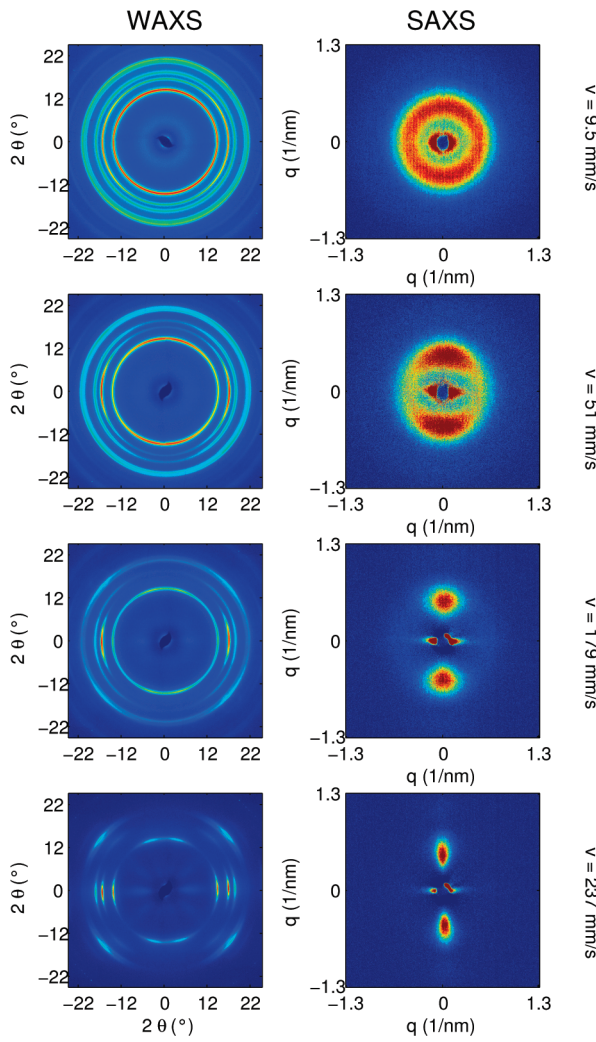


**Figure 6.** Examples of WAXS and SAXS measurements at polymer fibers with different take-up speeds when high molecular polymer is added.

Orientation parameter,  $\sigma$ , and radius,  $R$ , of the lamellas show that with additional long chains in the polymer we can reach higher orientation and far broader kebabs (Figures 7 and 9). In particular, the blended sample with a kebab-radius of  $R \approx 26$  nm shows a significant increase compared with the matrix material samples. Additionally, the blends show a stronger development than the matrix specimen.

We also analyzed the SAXS crystallinity  $X_C = H/L$  (Figure 8). We find that with increasing take-up speed, the crystallinity usually declines with saturation at higher velocities. The fraction of high molecular PP, however, does not seem to affect the results. To confirm this behavior, WAXS measurements have been done in Guinier setup. The crystallinity again first decreases with increasing take-up speed, as can be seen in Figure 8. As with SAXS measurements, the values saturate at high velocities. At increased take-up velocities, the SAXS crystallinity appears to be lower than the WAXS crystallinity. A possible explanation for this effect might be that the contribution of the shish to the crystallinity is not regarded in the simplified approach to SAXS crystallinity and that crystals grown perpendicular on the kebabs<sup>9–11</sup> do not appear in SAXS measurements.

Except for lamella radius and degree of orientation, almost all analyzed parameters show saturation at high take-up speeds. This behavior seems also to be independent of the molecular weight distribution.

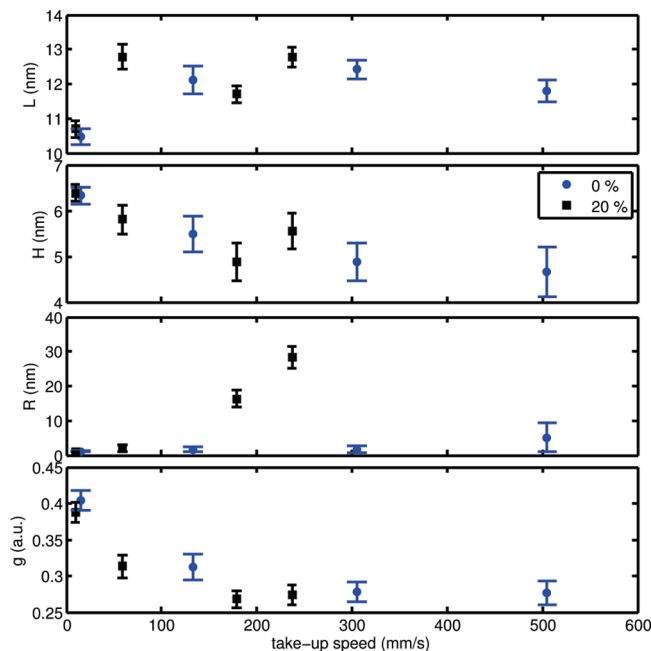


**Figure 7.** Long spacing,  $L$ , kebab height,  $H$ , radius,  $R$ , and lattice distortion,  $g$ , in polymer fibers, depending on take-up velocity and molecular weight distribution.

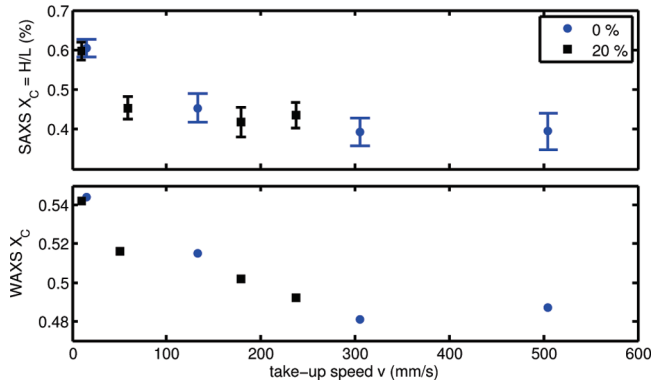


**Figure 8.** SAXS and WAXS crystallinity,  $X_C$ , of fibers, depending on the take-up velocity.

**WAXS Orientation in Melt-Spun Polypropylenes.** The degree of orientation of the crystalline phase was measured by WAXS (Figures 5 and 6) and evaluated with Hoseman's orientation function (Figure 9). The  $a'$  axes are usually randomly or slightly parallel oriented toward the fiber axis. This changes, however, for the fastest spun fiber with added high molecular polymer. Such a behavior indicates that the increased spinline stress at the highest take-up velocity decreases the amount of crystallites where the  $a'$  axis is aligned along the fiber direction. The WAXS scattering images of the spun fibers show that there are always contributions from two types of crystalline scattering where either the  $c$  axis or the  $a'$  axis is oriented along the spinning direction. This is in agreement with the common model for shish-kebab morphology.<sup>9–11</sup>

The orientation of the  $c$  axes steadily increases, whereas the  $b$  axes seem to orient already at low take-up speeds with only little increased orientation at higher speeds. This effect has already been observed by White et al. at very high take-up velocities with PPs comparable in molecular weight to our low molecular polymer.<sup>19</sup> They identified the spinline stress to be the significant parameter for orientation, crystallinity,

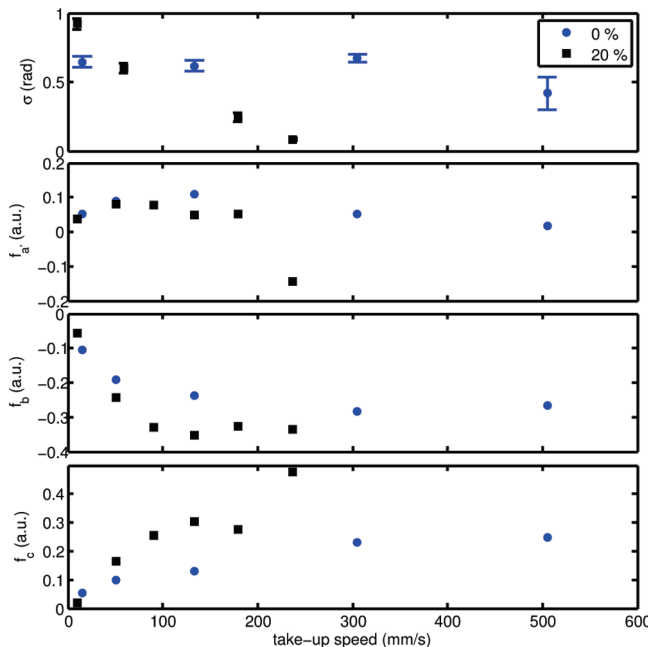


**Figure 9.** SAXS orientation parameter,  $\sigma$ , and Herman's orientation parameter,  $f$ , calculated for  $a'$ ,  $b$  and  $c$  axes from WAXS measurements.

and mechanical properties of the spun fibers. In their study, orientation and crystallinity increased with increasing spinline stress. We found a deviation from their results: crystallinity was reduced with higher spinline stresses. This deviation might be due to the much higher spinning speeds used in their work. It is therefore interesting to note that we got similar results for the orientation parameters in the blends with high molecular PP. Obviously, the long chains allow us to reduce the spinning speed while reaching even higher orientation. This might be interesting for industrial processing and applications.

Microscopic (SAXS) and crystalline (WAXS) orientation are compared in Figure 9. We should point out that it is not reasonable to compare the absolute values because in SAXS we use the width of the orientation distribution and in WAXS we use the expansion of the azimuthal peak function in Legendre polynomials as a measure for the degree of orientation. Therefore, we can only compare the results qualitatively. The orientation in the blends is usually more pronounced compared with the matrix polymer. We find the highest orientation in SAXS correlated with a distinctive orientation of the  $a'$  and  $c$  axes. Interestingly, the  $a'$  axes show an isotropic orientation for all other samples. It is noteworthy that the continuous growth of orientation in SAXS is matched by a successive orientation of the lattice planes. The  $b$  and  $c$  axes first align perpendicular and along to the stretching direction, respectively. Then, the  $a'$  and  $c$  axes show increasing orientation in a second step, which can only be observed in the blend. In between, we usually find plateaus for the respective lattice orientation in WAXS scattering. The rather flat curve progression of the matrix polymer in SAXS is met by the WAXS results on all lattice planes.

As discussed, we found that the  $b$  axis orients perpendicular to the fiber axis. The  $a'$  axis changes from isotropic to a pronounced perpendicular orientation only at high velocities and in the blend. The  $c$  axis is however oriented along the fiber axis. The chains (helices) are consequently also aligned along the fiber axis. This is in agreement with the common models for shish-kebab and lamella structures.<sup>2,3</sup>

## Summary

A model developed by Wilke<sup>34</sup> has been adapted to melt-spun fiber samples of PP. The evolving shish-kebab structure can be represented by cylinders in a paracrystalline lattice. To introduce the orientation of such clusters, the intensity function of one cluster as well as the orientation distribution function are expanded into Legendre coefficients. The intensity distribution of oriented clusters can then be obtained by a method proposed by Deas.<sup>42</sup> One of the distinct advantages of this model compared with other approaches is that the radius of the kebabs can be obtained besides their height and spacing. Furthermore, we can separate the contributions of orientation and lateral expansion of the scattering units.

We found that depending on the molecular weight distribution, we can get increased orientation and lamella radii. A growth of lamella diameters from  $\sim 10$  to  $> 50$  nm, as seen in one sample, has not been previously reported in the literature. We also compared the microscopic alignment on the lamella scale to the crystalline orientation. For the crystalline orientation, the Herman's orientation parameter has been calculated from WAXS data. Whereas the microscopic alignment seemed to be a continuous process, we found the crystalline orientation parameters changing in jumps and occurring at different lattice planes. The microscopic (lamella) orientation therefore corresponds to a series of crystalline alignments.

We will finally comment on the used approach to SAXS data evaluation. To our knowledge, this is the first work in the realm of SAXS on fibers using a direct model fitting approach. The presented model, connected to a direct fitting approach, allows us to evaluate up to seven structural parameters compared with the two to three parameters from peak analysis or other methods. Limitations of the model have been pointed out and will be addressed in future publications.

**Acknowledgment.** We thank Michael Stark and Professor Nicola Hüsing from the Institute of Inorganic Chemistry I of the University of Ulm for the SAXS measurements presented in this publications. Some of the WAXS measurements have been performed by Kay Egloff. Anke Leitner, Manuela Pluntke, and Christian Holzheu assisted by proofreading this manuscript.

**Supporting Information Available:** The presented model for shish-kebab or lamellar structures has been used for simulations of SAXS data to clarify the influence of the single parameters. We also added calculations regarding the influence of the single parameters on the peak position of the meridional reflexes and a description of the separation between orientation and lateral dimension of the lamellar stacks. Furthermore, we present some common structures found in semicrystalline polymers (like layer structures or sheared lamellas) and their explanation in the case of the proposed model.

This material is available free of charge via the Internet at <http://pubs.acs.org/>.

## References and Notes

- (1) Pasquini, N. *Polypropylene Handbook*; Carl Hanser Verlag: Munich, 2005.
- (2) Strobl, G. *The Physics of Polymers*; Springer: New York, 2007.
- (3) Keller, A.; Kolnaar, H. W. H. *Material Science and Technology: A Comprehensive Treatment*; VCH: New York, 1997.
- (4) Samon, J. M.; Schultz, J. M.; Hsiao, B. S.; Seifert, S.; Stribeck, S.; Gurke, I.; Collins, G.; Saw, C. *Macromolecules* **1999**, *32*, 8121.
- (5) Dukovski, I.; Muthukumar, M. *J. Chem. Phys.* **2003**, *118*, 6648–6655.
- (6) Wang, M.; Hu, W.; Ma, Y.; Ma, Y. *Macromolecules* **2005**, *38*, 2806–2812.
- (7) Nogales, A.; Hsiao, B. S.; Soman, R. H.; Srinivas, S.; Tsou, A. H.; Balta-Calleja, F. J.; Ezquerro, T. A. *Polymer* **2001**, *42*, 5247–5256.

- (8) Kimata, S.; Sakurai, T.; Nozue, Y.; Kasahara, T.; Yamaguchi, N.; Karino, T.; Shibayama, M.; Kornfield, J. A. *Science* **2007**, *316*, 1014–1017.
- (9) Fujiyama, M.; Wakino, T.; Y., K. *J. Appl. Polym. Sci.* **1988**, *35*, 29–49.
- (10) Schrauwen, B. A. G.; v. Breemen, C. A., L.; Spoelstra, A. B.; Govaert, L. E.; Peters, G.W. M.; Meijer, H. E. H. *Macromolecules* **2004**, *37*, 8618–8633.
- (11) Zhu, P.-W.; Graham, E. *J. Mater. Sci.* **2008**, *43*, 6459–6467.
- (12) Dees, J. R.; Spruiell, J. E. *J. Appl. Polym. Sci.* **1974**, *18*, 1053–1078.
- (13) Guinier, A.; Fournet, G. *Small-Angle Scattering of X-rays*; Wiley: New York, 1955.
- (14) Glatter, O.; Kratky, O. *Small Angle X-ray Scattering*; Academic Press: London, 1982.
- (15) Balta-Calleja, F. J.; Vonk, C. G. *X-ray Scattering of Synthetic Polymers*; Elsevier: New York, 1989.
- (16) Stribeck, N. *X-ray Scattering of Soft Matter*; Springer: New York, 2007.
- (17) Schneider, K.; Zafeiropoulos, N. E.; Stamm, M. *Adv. Eng. Mater.* **2009**, *11*, 502–506.
- (18) Ellison, M. S.; Lopes, P. E.; Pennington, W. T. *J. Eng. Fibers Fabr.* **2008**, *3*, 10–21.
- (19) Nadella, H. P.; Henson, H. M.; Spruiell, J. E.; White, J. L. *J. Appl. Polym. Sci.* **1977**, *21*, 3003–3022.
- (20) Huda, M. N.; Bauer, S.; Dragaun, H.; Skalicky, P. *Colloid Polym. Sci.* **1984**, *262*, 110–114.
- (21) Kolb, R.; Seifert, S.; Stribeck, N.; Zachmann, H. *Polymer* **2000**, *41*, 1497–1505.
- (22) Bankar, V.; Spruiell, J. E.; White, J. L. *J. Appl. Polym. Sci.* **1977**, *21*, 2135–2155.
- (23) Danford, M. D.; Spruiell, J. E.; White, J. L. *J. Appl. Polym. Sci.* **1978**, *22*, 3351–3361.
- (24) Cakmak, M.; Kim, J. C. *J. Appl. Polym. Sci.* **1997**, *64*, 729–747.
- (25) Samon, J. M.; Schultz, J. M.; Hsiao, B. S.; Khot, S.; Johnson, H. R. *Polymer* **2001**, *42*, 1547–1559.
- (26) White, J. L.; Cakmak, M. *Adv. Polym. Technol.* **1986**, *6*, 295–337.
- (27) Kitao, T.; Spruiell, J. E.; White, J. L. *Polym. Eng. Sci.* **1979**, *19*, 761–773.
- (28) Schultz, J. M.; Hsiao, B. S.; Samon, J. M. *Polymer* **2000**, *41*, 8887–8895.
- (29) Dencheva, N.; Nunes, T. G.; Oliveira, M. J.; Denchev, Z. *J. Polym. Sci., Part B: Polym. Phys.* **2005**, *43*, 3720–3733.
- (30) Nozue, Y.; Shinohara, Y.; Ogawa, Y.; Sakurai, T.; Hori, H.; Kasahara, T.; Yamaguchi, N.; Yagi, N.; Amemiya, Y. *Macromolecules* **2007**, *40*, 2036–2045.
- (31) Murthy, N. S.; Zero, K.; Grubb, D. T. *Polymer* **1997**, *38*, 1021–1028.
- (32) Murthy, N. S.; Grubb, D. T. *J. Polym. Sci., Part B: Polym. Phys.* **2002**, *40*, 691–705.
- (33) Murthy, N. S. *Rigaku J.* **2004**, *21*, 15–24.
- (34) Wilke, W.; Göttlicher, K. *Colloid Polym. Sci.* **1981**, *259*, 596–601.
- (35) Göttlicher, K.; Fronk, W.; Wilke, W. *Colloid Polym. Sci.* **1983**, *261*, 126–132.
- (36) Wilke, W. *Acta Crystallogr., Sect. A* **1983**, *39*, 864–867.
- (37) Göttlicher, K. Diploma Thesis, Universität Ulm, **1981**.
- (38) Fronk, W.; Wilke, W. *Colloid Polym. Sci.* **1983**, *261*, 1010–1021.
- (39) Fronk, W. Ph.D. Thesis, Universität Ulm, **1984**.
- (40) Fronk, W.; Wilke, W. *Colloid Polym. Sci.* **1985**, *97*, 263.
- (41) Fronk, W. *J. Polym. Sci., Part B: Polym. Phys.* **1986**, *24*, 839–856.
- (42) Deas, H. D. *Acta Crystallogr.* **1952**, *5*, 542.
- (43) A 100% high molecular sample could not be extruded because of the increased viscosity of the material.
- (44) Ward, I. M. *Structure and Properties of Oriented Polymers*; Applied Science Publishers: London, 1975.
- (45) Wilchinsky, Z. W. *J. Appl. Phys.* **1960**, *31*, 1969–1972.
- (46) Stein, R. S. *J. Polym. Sci.* **1958**, *31*, 327–334.
- (47) Because of the symmetry of the scattering pattern, we evaluated the azimuthal slice only between  $\theta^* = 0$  and  $\pi$ .
- (48) Hosemann, R.; Bagchi, S. N. *Direct Analysis of Diffraction by Matter*; North-Holland: Amsterdam, 1962.
- (49) Hosemann, R.; Vogel, W.; Weick, D.; Baltá-Calleja, F. J. *Acta Crystallogr., Sect. A* **1981**, *37*, 85–91.
- (50) When we are dealing with semicrystalline polymers, we can presume a “paracrystalline lattice”. This means that the crystalline lattice finds itself subjected to distortions of the second kind (distortions of the first kind describe a situation where the objects are still in a regular lattice but vary around their designated position as given with random thermal displacements): Starting from a chosen origin the next neighbors distance is not constant but varying. Different distributions for the distance function have been proposed in literature. Crist has shown that usually a symmetric or slightly skewed distribution is best suited to describe the actual SAXS data.<sup>60,61</sup> We therefore used a Gaussian distribution for the next neighbor distance. The whole lattice builds on the varying distance principle; therefore, we loose all long-range order, and higher order reflections in scattering experiments are usually negligible. This can also be observed in semicrystalline polymers. A significant advantage of this model is that it can be analyzed analytically: the lattice factor can be directly calculated as the absolute squared of the Fourier transform of such a lattice.<sup>38,40,48</sup>
- (51) Förster, S.; Timmann, A.; Konrad, M.; Schellbach, C.; Meyer, A.; Funari, S. S.; Mulvaney, P.; Knott, R. *J. Phys. Chem. B* **2005**, *109*, 1347–1360.
- (52) Wilke, W.; Bratrich, M.; Heise, B.; Peichel, G. *Polym. Adv. Technol.* **1992**, *3*, 179–190.
- (53) Hobbs, J. K.; Miles, M. J. *Macromolecules* **2001**, *34*, 353–355.
- (54) A closer analysis of the simulations has shown that with increasing orientation the scattering profile of the complete orientation model and a simplified model without orientation on the meridian become similar. We can therefore ignore the scattering contribution of the radial part and use the simplified model for a faster fit of the parameters  $L$ ,  $g$ , and  $H$ .
- (55) Bevington, P. R.; Robinson, K. D. *Data Reduction and Error Analysis for the Physical Sciences*; McGraw-Hill: Boston, 2002.
- (56) Alexander, L. E. *X-ray Diffraction Methods in Polymer Science*; Wiley-Interscience: New York, 1969.
- (57) Murthy, N. S.; Bednarczyk, C.; Moore, R. A. F.; Grubb, D. T. *J. Polym. Sci., Part B: Polym. Phys.* **1996**, *34*, 821–835.
- (58) Men, Y.; Rieger, J.; Lindner, P.; Enderle, H.-F.; Lilge, D.; Kristen, M. O.; Mihan, S.; Jiang, S. *J. Phys. Chem. B* **2005**, *109*, 16650–16657.
- (59) Samon, J. M.; Schultz, J. M.; Hsiao, B. S. *Polymer* **2000**, *41*, 2169–2182.
- (60) Crist, B. *J. Polym. Sci., Polym. Phys. Ed.* **1973**, *11*, 635–661.
- (61) Crist, B.; Morosoff, N. *J. Polym. Sci., Polym. Phys. Ed.* **1973**, *11*, 1023–1045.